Cancer Cell
Article

Inducible FGFR-1 Activation Leads to Irreversible Prostate Adenocarcinoma and an Epithelial-to-Mesenchymal Transition

Victor D. Acevedo,[1,2] Rama D. Gangula,[2] Kevin W. Freeman,[1,2] Rile Li,[3] Youngyou Zhang,[5] Fen Wang,[5] Gustavo E. Ayala,[3] Leif E. Peterson,[4] Michael Ittmann,[3] and David M. Spencer[1,2,*]
[1]Program in Cell and Molecular Biology
[2]Department of Immunology
[3]Department of Pathology
[4]Department of Medicine
Baylor College of Medicine, One Baylor Plaza, Houston, TX 77030, USA
[5]Texas A&M University Health Science Center, Houston, TX 77030, USA
*Correspondence: dspencer@bcm.edu
DOI 10.1016/j.ccr.2007.11.004

SUMMARY

Fibroblast Growth Factor Receptor-1 (FGFR1) is commonly overexpressed in advanced prostate cancer (PCa). To investigate causality, we utilized an inducible FGFR1 (iFGFR1) prostate mouse model. Activation of iFGFR1 with chemical inducers of dimerization (CID) led to highly synchronous, step-wise progression to adenocarcinoma that is linked to an epithelial-to-mesenchymal transition (EMT). iFGFR1 inactivation by CID withdrawal led to full reversion of prostatic intraepithelial neoplasia, whereas PCa lesions became iFGFR1-independent. Gene expression profiling at distinct stages of tumor progression revealed an increase in EMT-associated *Sox9* and changes in the Wnt signaling pathway, including *Fzd4*, which was validated in human PCa. The iFGFR1 model clearly implicates FGFR1 in PCa progression and demonstrates how CID-inducible models can help evaluate candidate molecules in tumor progression and maintenance.

INTRODUCTION

Despite improvements in prostate cancer (PCa) management, an estimated 27,050 U.S. men will die of PCa in 2007 (Jemal et al., 2007), underscoring the need for a more thorough molecular understanding of this resilient disease. Significant progress has been made in the identification of molecular markers, growth factors, and other proto-oncogenes that may be involved in PCa (Bradford et al., 2006). In particular, members of the fibroblast growth factor family and their receptors are known to be highly misregulated (Kwabi-Addo et al., 2004; Powers et al., 2000). Although FGF receptor 1 (FGFR1) is not normally expressed in benign prostate epithelium, it is upregulated in about 40% of poorly differentiated prostate adenocarcinomas, suggestive of a causal role in disease progression (Ozen et al., 2001; Giri et al., 1999; Naimi et al., 2002).

FGFR1 is part of a group of growth factor receptor tyrosine kinases (RTK) able to induce several tumorigenic processes, including cell proliferation, angiogenesis, inhibition of apoptosis, and cell migration (Grose and Dickson, 2005). RTKs have also been proposed to provide resistance to cytotoxic therapies that are based on DNA

SIGNIFICANCE

Receptor tyrosine kinases (RTKs) can promote a range of cellular processes that can lead to tumorigenesis, making RTKs a good therapeutic target. Development of appropriate RTK-based models that progress to prostate cancer could facilitate elucidation of both pathological changes during progression and potential therapies. Herein, we show that prolonged activation of inducible FGFR1 (iFGFR1) signaling is sufficient for step-wise progression to invasive PCa. This conditional, reversible model facilitated the identification of temporal differences in responsiveness to iFGFR1 inhibition indicative of a "susceptibility window" for targeting FGFR1. Gene expression profiling further permitted identification of candidate molecules that can potentially differentiate FGFR1-dependent and -independent stages. This model provides a platform to test single or FGFR1-combined therapies and a proof-of-principal for similar reversible models.

damage and apoptosis by inducing repair of DNA lesions (Skorski, 2002). Another mechanism by which FGFR1 and other RTKs are believed to induce tumorigenesis is by disrupting normal epithelial/stromal communication. In the prostate, homeostasis can be maintained, at least partly, by paracrine signaling between stromal cells, which produce FGF7 and FGF10 and proximal epithelial cells, expressing their cognate FGFR isoform, FGFR2iiib (Ornitz et al., 1996). During PCa progression, alternative splicing of FGFR2 can occur in epithelial cells, leading to isoform changes from FGFR2iiib to the more ligand promiscuous FGFR2iiic, along with ectopic expression of typically stroma-localized FGFR1iiic, potentially destroying the balanced interdependence between stroma and epithelium (Carstens et al., 1997; Feng et al., 1997). Because the prostate microenvironment is enriched with FGFR1 ligands such as FGF2, changes in the FGFR axis are thought to trigger autocrine signaling and stromal-independence (Kwabi-Addo et al., 2004). Moreover, FGF2 is highly upregulated in PCa and can support tissue remodeling via its proangiogenic properties (Giri et al., 1999).

The development of genetically engineered mouse (GEM) PCa models can help dissect the role of the FGF axis in disease progression in a physiological setting. In particular, GEM models facilitate the study of initiation and stepwise progression of disease within the context of the prostate microenvironment. Furthermore, performing experiments in an immunocompetent organism can illustrate the role that stromal leukocytes can have on disease progress, better recapitulating human disease (Shappell et al., 2004). One of the obstacles in sorting out the distinct roles of disparate FGF axis molecules has been that many of the 22 known FGF ligands, 4 highly promiscuous FGFRs, and their isoforms are typically coexpressed in the same tissue (Ornitz and Itoh, 2001). To overcome this challenge, our lab developed a GEM model based on targeted, inducible FGFR1 (iFGFR1) activation, named the *j*uxtaposition *o*f *C*ID and *k*inase1 (JOCK1) model (Freeman et al., 2003). Expression of iFGFR1 was directed to prostate epithelial cells by the use of the composite probasin promoter, ARR_2PB (Zhang et al., 2000). Upon treatment with a synthetic, lipid-permeable chemical inducer of dimerization (CID), prostate-localized iFGFR1 can oligomerize, leading to activation of FGFR1 signaling. Previously, we observed that mice treated biweekly with CID for 12–24 weeks progressed to mPIN and that early hyperplastic changes are largely reversible after CID withdrawal (Freeman et al., 2003).

The FGF signaling axis also plays an important role during early stages of embryonic development, such as gastrulation. FGFR1 is known to drive an epithelial-to-mesenchymal transition (EMT) of primitive streak-localized epiblast cells into mesoderm cells (Ciruna and Rossant, 2001). In an EMT, epithelial cells lose their polarity, increase their motility, and begin to express mesenchymal markers, such as vimentin, becoming "mesenchymal-like." This process has also been linked to cancer progression, in which epithelial cells lose differentiation markers, such as E-cadherin, and acquire increased migratory capacity, leading to stromal invasion and metastasis (Thiery, 2002). EMTs are also associated with heterogeneous tumors with features of both carcinomas and sarcomas. These uncommon neoplasms are commonly referred to as sarcomatoid carcinomas (Thiery, 2002). In addition, the isoform switch from epithelial-type FGFR2IIIb to mesenchymal-type FGFR2IIIc, along with ectopic FGFR1 expression, has been postulated to be a manifestation of an EMT (Savagner et al., 1994; Yan et al., 1993). In a 3D mammary epithelial cell model based on mammary gland targeting, iFGFR1 was shown to drive an EMT associated with mesenchymal marker expression by inducing MMP3 expression and reducing E-cadherin levels, leading to increased cell motility (Xian et al., 2005).

Herein, we utilized the JOCK1 mouse model to test whether prolonged FGFR1 activation could lead to PCa. We found that after 42 weeks of CID treatment, JOCK1 mice consistently (100%) developed prostate adenocarcinoma, which were largely sensitive to androgen ablation. Additionally, we tested the effects of iFGFR1 inhibition by CID withdrawal at various times during cancer progression and observed that the mPIN phenotype can completely regress to normal within 8 months. Moreover, even relatively late withdrawal of iFGFR1 signaling can also significantly reduce proliferation and progression of adenocarcinoma. These results help to define a "susceptibility window" for pharmaceutical targeting of the FGFR axis. The use of gene expression microarrays allowed us to identify and validate several candidate molecules that can potentially differentiate early stages from late/nonreversible PCa. Finally, the development of sarcomatoid carcinomas, composed of both spindle-shaped and epithelial cells in JOCK1 mice, is strong evidence of an iFGFR1-mediated EMT. Collectively, these results reveal the potential roles of FGFR1 in tumor initiation, maintenance, and progression at different stages of cancer progression. Thus, JOCK1 mice can facilitate study of FGFR1 effects in PCa progression and are, to date, the only GEM model based on the FGF signaling axis which displays full penetrance to PCa.

RESULTS

Prolonged iFGFR1 Signaling Leads to Prostate Adenocarcinoma

Prostate cancer progression in humans is divided into several stages, progressing from preinvasive hyperplasia and prostatic intraepithelial neoplasia (PIN) to invasive adenocarcinoma and metastasis. Initial studies based on the JOCK1 GEM model concluded that 12–24 weeks of iFGFR1 signaling is sufficient to initiate PCa progression (Freeman et al., 2003). However, invasive adenocarcinoma was not apparent. To determine if iFGFR1 activation can lead to invasive adenocarcinoma or if FGFR1 signaling is somehow "self-limiting," JOCK1 mice were treated biweekly for 32, 42, or 52 weeks with CID (AP20187, 2 mg/kg). Following treatment, the genitourinary (GU) tracts, comprised of bladder, seminal vesicles, urethra,

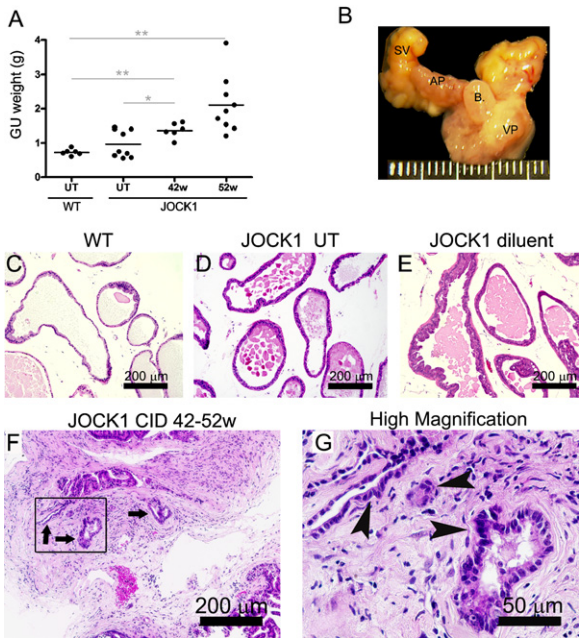

Figure 1. Extended iFGFR1 Activation Leads to Invasive Adenocarcinoma

(A) FGFR1 leads to an increase in genitourinary weight distribution of JOCK1 CID treated mice for 42 (n = 6) and 52 weeks (n = 9) in comparison to untreated (UT) wild-type (n = 6), UT JOCK1 mice (n = 9) (t test, $^{*}p < 0.05$, $^{**}p < 0.01$).

(B) Macroscopic view of typical JOCK1 prostate after 52 weeks of treatment.

(C–E) H&E analysis of age-matched wild-type (C), JOCK1 untreated (D), and JOCK1 52 weeks (E) vehicle shows a normal ventral prostate phenotype.

(F) JOCK1 mice treated with CID for 42–52 weeks showing areas of invasive cancer.

(G) Higher magnification of (F) showing small invasive glands (arrow) with hyperchromatic, atypic nuclei (arrowhead).

and all four prostate lobes, were initially removed and weighed. By 42 weeks of treatment, there was a highly significant increase in the mean GU tract size that was even larger by week 52 relative to age-matched, JOCK-1 littermates (Figures 1A and 1B). Moreover, after 52 weeks of CID administration, some mice began to develop several fluid-filled prostatic cysts, which may have contributed to some of the observed changes. Thus, prolonged CID-mediated iFGFR1 activation leads to a large increase in prostate/GU tract size.

To determine if the increase in prostate and GU tract size correlated with progression to PCa, we analyzed prostate tissue sections histologically. Wild-type, untreated JOCK1 and 52-week vehicle-treated JOCK1 mice, which were age-matched to 52-week-treated JOCK1 mice, exhibited a normal phenotype with limited age-associated focal hyperplasia (Figures 1C–1E). In contrast, JOCK1 mice treated with CID for 32 weeks had predominant mPIN, an adenocarcinoma precursor defined by nuclear atypia along with cribiform structures and cellular tufting within intact prostate glands. Mice also began to show signs of invasive epithelial cells and glandular atrophy. From 42 weeks onward, mice developed highly synchronized and penetrant adenocarcinoma in all lobes. These lesions were characterized by the presence of invasive hyperchromatic epithelial cells with prominent nucleoli and nuclear atypia along with the formation of multiple small invasive glands within desmoplastic stroma (Figures 1F and 1G). Taken together, these results show that activation of iFGFR1 in prostate epithelial cells, and not just its ectopic expression, leads to malignant transformation of JOCK1 prostates.

In order to better characterize the nature of JOCK1 tumors, we performed immunohistochemistry (IHC) analysis. In normal prostate glands, epithelial cells are surrounded by a layer of smooth muscle α-actin (SMA) expressing cells, which is lost as glandular cells become malignant. Mice with a normal prostate had an intact SMA layer surrounding the glands (Figure 2A). In comparison, after 32 weeks of CID treatment, JOCK-1 mice exhibited a loss of the surrounding SMA layer (Figure 2B), indicative of invasion.

One common characteristic of some PCa mouse models that express SV40 large T-antigen is the development of tumors with increased neuroendocrine (NE) cell characteristics (Shappell et al., 2004). In contrast, prostate tumors containing a large proportion of NE-like cells are rare in humans. To determine if JOCK1 tumors are epithelial cell derived, we examined the expression of common epithelial and NE cell markers. IHC revealed cytokeratin expression in JOCK1 tumors, indicative of invasive epithelial cells. Furthermore, within these lesions there are regions displaying a gradual loss of cytokeratin expression, suggesting that these cells have begun to lose some of their epithelial characteristics (Figure 2C). Androgen receptor (AR) is expressed primarily by secretory epithelial cells and not normally NE cells and plays an essential role in prostate development, cell proliferation, and inhibiting apoptosis. In the JOCK1 model, AR staining was primarily nuclear within invasive cells, consistent with AR activation in epithelial cells (Figure 2D). In contrast, JOCK1 tumors were negative for the NE marker synaptophysin (Figures 2E and 2F). Finally, since growth factor receptors can activate a variety of downstream signaling pathways, we analyzed Akt activation by iFGFR1. Six hours after CID administration, iFGFR1 triggered Akt phosphorylation and nuclear localization (Figures 2G and 2H). Along with reported MAPK activation (Freeman et al., 2003), iFGFR1 can activate downstream signaling pathways that can lead to epithelial-derived prostate tumors, indicative of invasive adenocarcinoma and not NE carcinoma.

FGFR1 Activity Leads to Heterogeneous Prostate Cancer

Treated JOCK1 mice not only developed well-differentiated adenocarcinoma, but also exhibited several distinct malignant phenotypes. To quantitate and better characterize the distribution of these phenotypes, JOCK1 tissues were independently analyzed by two pathologists and the extent of each tumor type scored from 0–3 according to proportion of each phenotype. The most predominant phenotypes

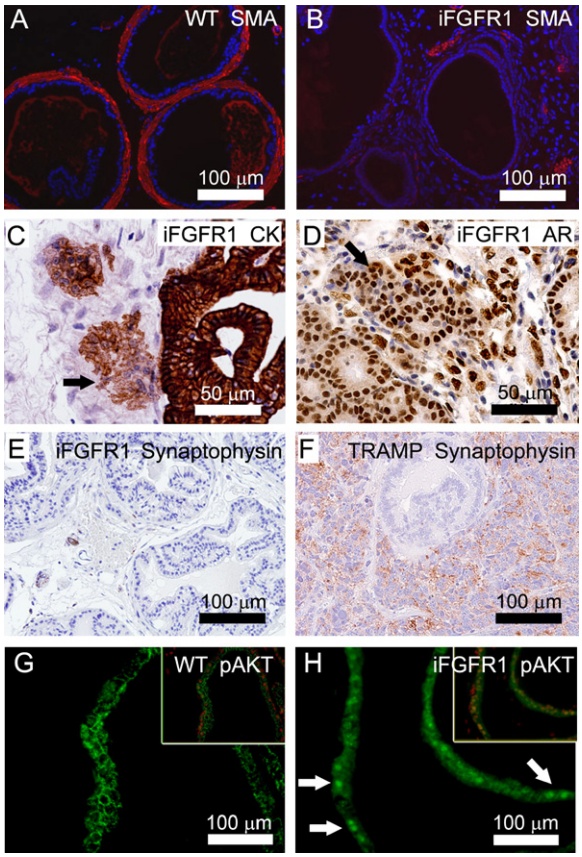

Figure 2. Immunohistochemical Characterization of JOCK1 Tumors

(A and B) Wild-type mice maintain a complete smooth muscle α-actin (red) layer surrounding prostate glands (A), while consistent with cell invasion, JOCK1 mice lose surrounding smooth muscle layer after 32 weeks of CID (B).

(C) Expression of epithelial marker pan-cytokeratin (CK) is reduced by invasive cells (arrow).

(D) iFGFR1 tumors display high nuclear androgen receptor in both glandular epithelial cells and invasive cells.

(E and F) Expression of neuroendocrine marker synaptophysin in TRAMP, but not JOCK1, tumors.

(G and H) iFGFR1 leads to an increase in Akt phosphorylation and nuclear localization in comparison to WT mice. Insert shows nuclear staining with DAPI pseudocolored red.

described were mPIN (Figure 3A), adenocarcinoma (Figures 1F and 1G), transitional sarcomatoid-carcinoma (TS) (Figures 3B and 3C), and frank sarcoma (Figure 3D). Transitional sarcomatoid lesions were characterized by a mixture of poorly differentiated epithelial cells with atypical nuclei and spindle-shaped cells around prostate carcinoma glands. Sarcomas present were composed of spindle-shaped cells appearing to have formed from TS lesions. The average scores from both pathologists were taken and graphed according to treatment time and phenotype (Figure 3E). Analysis of age-matched wild-type mice and JOCK1 control mice did not reveal any of these four phenotypes; rather, they appeared normal. JOCK1 mice treated for 32 weeks exhibited primarily mPIN, with some signs of PCa and TS lesions. By 42 weeks of treatment, all (100%) mice developed PCa, and the extent of adenocarcinoma increased with prolonged treatment. Furthermore, the extent of TS lesions increased with treatment, becoming frequent after 42 weeks, correlative with PCa development. This suggests that TS lesions may be dependent on epithelial cell invasion. Although JOCK1 mice also developed sarcomas, this was relatively rare and the rate did not seem to increase over time, suggesting that this event may require additional stochastic cellular changes. Therefore, extended iFGFR1 activity leads to the development of sarcomatoid carcinoma-like tumors, suggestive of a role of FGFR1 in an epithelial-to-mesenchymal transition in transformed epithelial cells or, alternatively, an increase in mesenchymal cell proliferation.

FGFR1 Leads to an EMT and Distant Metastasis

The presence of atypical spindle-shaped cells surrounding epithelial cells led to the hypothesis that these morphologically mesenchymal-like cells may have had epithelial progenitors and undergone an EMT. One of the challenges in identifying a true EMT is its transient nature. Reduction in the levels of traditional epithelial markers as cells become less differentiated can add to the problem (Thiery, 2002). To test faux EMT, serial sections of iFGFR1 tumors exhibiting characteristics of both carcinomas and sarcomas (i.e., TS tumors) were stained by H&E and IHC for AR, E-cadherin, and cytokeratin expression (Figures 4A–4D). Mesenchymal-like cells exhibited nuclear AR expression, similar to epithelial cells (Figure 4B). Another epithelial marker, E-cadherin, localizes to the plasma membrane, playing a well-established role in cell adhesion. In TS tumors, differentiated epithelial cells maintained E-cadherin membrane localization. In contrast, invasive morphologically mesenchymal-like cells expressed lower and more diffuse levels of E-cadherin (Figure 4C), and a high percentage of these mesenchymal-like cells have loss of cytokeratin expression associated with loss of epithelial differentiation (Figure 4D). At the same time, double IF staining showed a high percentage of these spindle-shaped cells had high expression of the mesenchymal marker vimentin in contrast to adjacent glandular epithelial cells, which retained E-cadherin expression (Figure 4E). Interestingly, we also observed a rare subset of cells showing coexpression of E-cadherin and vimentin between epithelial and mesenchymal cells, consistent and indicative of the transient nature of an EMT (Figure 4F). As expected, frank sarcoma lesions displayed widespread vimentin (Figure 4G) with very low cytokeratin and E-cadherin expression (see Figure S1 in the Supplemental Data available with this article online) while maintaining nuclear AR expression, suggesting that these cells may be epithelial cell derived, and later dedifferentiated into mesenchymal-like cells, likely by an EMT (Figure 4H). Thus, the JOCK-1 model shows the hallmarks of an EMT with the full spectrum of cancer progression from adenocarcinoma to frank sarcoma.

Previous studies have proposed a mechanism in which FGFR1, by controlling the expression levels of the

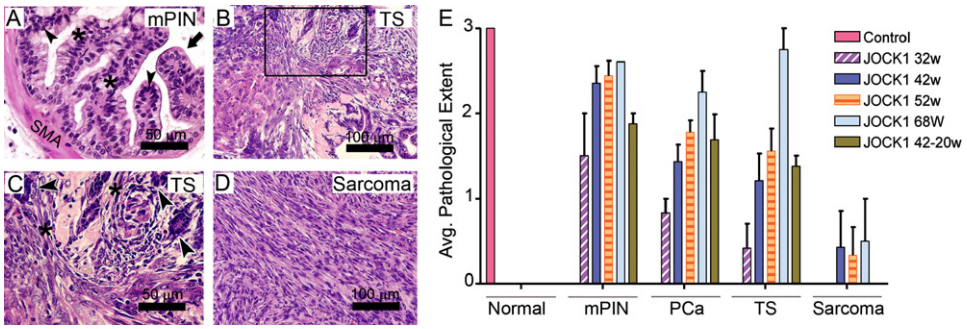

Figure 3. Pathological Grading of JOCK1 Tumors

(A–D) Prolonged iFGFR1 activation leads to adenocarcinoma and distinct phenotypes: (A) mPIN, defined by complex cribiform arrangement (*) with papillary structures (arrow), hyperchromatic atypical nuclei, some of which have prominent nucleoli (arrowhead), and an intact smooth muscle layer reflecting lack of invasion (SM); (B) transitional sarcomatoid-carcinoma (TS) and higher magnification (C) characterized by invasive carcinoma cells (arrow head) surrounded by spindle-shaped cells (*); and (D) sarcomas, comprised of organized spindle-shaped cells.

(E) Shows the average pathological extent for the distribution of mPIN, adenocarcinoma, transitional sarcomatoid, and sarcoma phenotype per sample. Phenotypes were grouped and graphed according to wild-type or JOCK1 mice treatment. Results show that only age-matched wild-type mice and JOCK1 untreated (control) mice exhibit a normal phenotype. After 42 weeks of treatment, 100% of JOCK1 mice developed adenocarcinoma. JOCK1 mice treated for 42 weeks followed by 20 weeks of CID withdrawal show an average PCa and sarcomatoid extent higher than 42-week treated mice, but lower than continuously treated mice. Represented as mean ± SEM.

transcriptional repressor Snail, leads to an EMT during embryonic development (Ciruna and Rossant, 2001). This short-lived zinc finger family member is known to reduce E-cadherin transcription levels (Zhou et al., 2004). Nevertheless, iFGFR1 did not lead to a significant increase in *Snail1* mRNA in prostate epithelial cells, but Snail1/2 protein was found to be expressed in several foci in JOCK1 tumors (Figures 4I and 4J). Thus, a combination of other factors may be required for FGFR1 induction of Snail1 expression.

One of the properties that an EMT confers is an increase in migratory capacity, which contributes to metastasis. However, distant metastases were not commonly found in tumor-bearing JOCK1 animals. Yet, despite the low frequency, JOCK1 mice that developed sarcomas did show evidence of distant metastasis by 42 weeks of CID. Spindle-shaped cells were found in the liver and lymph nodes (Figure 4K). To test if these cells were derived from prostate tumors, we looked for the expression of AR and cytokeratins. Positive nuclear AR staining was found only in metastatic cells but not in hepatocytes or lymphocytes. Cytokeratin expression was also found in a subset of metastatic spindle-shaped cells in the liver. These metastatic cells did not express E-cadherin, consistent with loss of cell adhesion and increased migration. Taken together, these results show that these spindle-shaped cells may have had a prostate epithelial origin and subsequently lost most of their epithelial characteristics as they became less differentiated or more mesenchymal-like, ultimately developing into highly malignant tumors with a propensity for metastasis.

Deactivation of iFGFR1 Signaling by CID Withdrawal Leads to Regression of Low-Grade PIN and Reduces Prostate Adenocarcinoma Progression

To determine if prolonged iFGFR1 signaling is necessary for tumor maintenance, we took advantage of the CID system's ability to terminate iFGFR1 signaling by CID withdrawal. Previous JOCK1 studies showed that prostates developing hyperplasia, but not those progressing to mPIN, were able to completely regress after 8 weeks of CID withdrawal (Freeman et al., 2003). However, we could not rule out that an even longer period was necessary for the regression of iFGFR1-mediated mPIN. Alternatively, changes in prostate microenvironment, such as an increase in neovascularization, could have led to iFGFR1-independent changes or cancer progression. To address these possibilities, iFGFR1 activity was terminated for 18–20 weeks after JOCK1 mice had been treated for 12 or 42 weeks to affect the development of mPIN or PCa, respectively. Mice that developed mPIN after 12 weeks of treatment contained glands completely filled with cells (Figure 5A). However, by 18 weeks of CID withdrawal, JOCK1 prostates began to show signs of reversion (n = 3) (Figure 5B). To test if a longer CID latency period could allow for full reversion, a larger cohort (n = 7) was examined. After 36 weeks of drug withdrawal, 12-week-treated JOCK1 mice had almost full mPIN reversion, excluding some focal hyperplasia typical of aged mice (Figure 5C). This delay in regression may be due to the slow reversion of neovascularization seen after CID withdrawal (Winter et al., 2007). Thus, terminating iFGFR1 activity once mPIN has developed demonstrates that FGFR1 is necessary for both mPIN maintenance and further progression, and that even initial neoplastic changes can revert to normal after a longer period of iFGFR1 deactivation.

In contrast to JOCK1 mice that developed mPIN, 42 week treated JOCK1 mice displaying adenocarcinoma did not show significant signs of reversion after 20 weeks of CID withdrawal (n = 5). These mice contained more neoplastic prostates relative to mice treated for 42 weeks (Figures 5D and 5E). The average pathological extent of adenocarcinoma in mice treated for 42 weeks followed by a 20-week CID withdrawal period was higher than

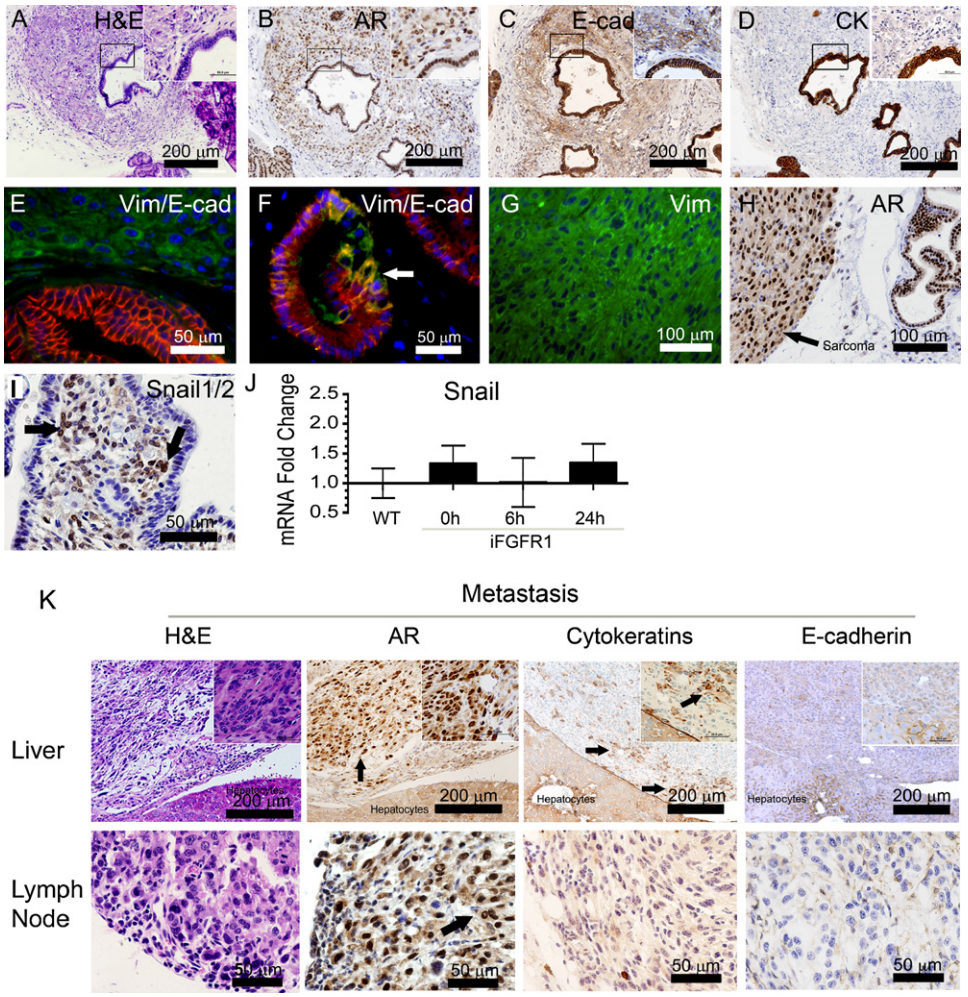

Figure 4. Long-Term iFGFR1 Signaling Leads to an EMT in PCa Progression

(A–D) Serial sections of transitional sarcomatoid. (A) H&E staining of transitional sarcomatoid, both epithelial cells and surrounding mesenchymal-like cells expressed nuclear AR (B). (C) Mesenchymal-like cells retained E-cadherin expression, and (D) loss of cytokeratin (CK) expression among mesenchymal-like cells.

(E) Sarcomatoid-carcinoma lesion, with mesenchymal-like cells expressing the mesenchymal marker vimentin (green) adjacent to epithelial cells expressing E-cadherin (red).

(F) Coexpression of vimentin (green) and E-cadherin (red) within epithelial and mesenchymal cells is indicative of a transient EMT.

(G) Sarcoma lesions express vimentin.

(H) Expression of androgen receptor by both sarcoma and glandular epithelial cells.

(I) EMT-associated Snail1 nuclear expression.

(J) iFGFR1 does not lead to a direct increase in Snail1/2 mRNA (1-way ANOVA represented as mean ± SEM).

(K) Metastatic spindle-shaped cells within the liver and lymph nodes stained by H&E and IHC for AR, Cytokeratin, and E-cadherin. Expression of cytokeratin by metastatic mesenchymal-like cells is suggestive of sarcomatoid phenotype.

JOCK1 mice treated for 42 weeks, but not as high as mice treated continuously for 52 to 68 weeks (Figures 3E and 5F), suggesting that both iFGFR1-dependent and -independent changes can occur after adenocarcinoma is established. Thus, in comparison with JOCK1 mice that progress to mPIN, inhibition of iFGFR1 does not allow for regression of PCa but can still slow the rate of progression when compared to continuously treated JOCK1 mice. Furthermore, when mice were treated using androgen ablation, there was also a difference in susceptibility between mPIN and PCa (Figure S2). Similar to human cancer, tumors were initially responsive to therapy, but signs of androgen independence begin to arise in a subset of mice with PCa.

To further address the effects of iFGFR1 signaling inhibition, proliferation rates were examined by staining for proliferation marker Ki-67 (Figures 5G–5J). Mice that were treated for 12 weeks had about 7.5% Ki-67 positive cells, but following CID withdrawal after 18 and 36 weeks, the proportion of proliferating cells dropped significantly to ~2% (Figure 5K). Furthermore, there was a reduction in the level of proliferation from JOCK1 mice treated with

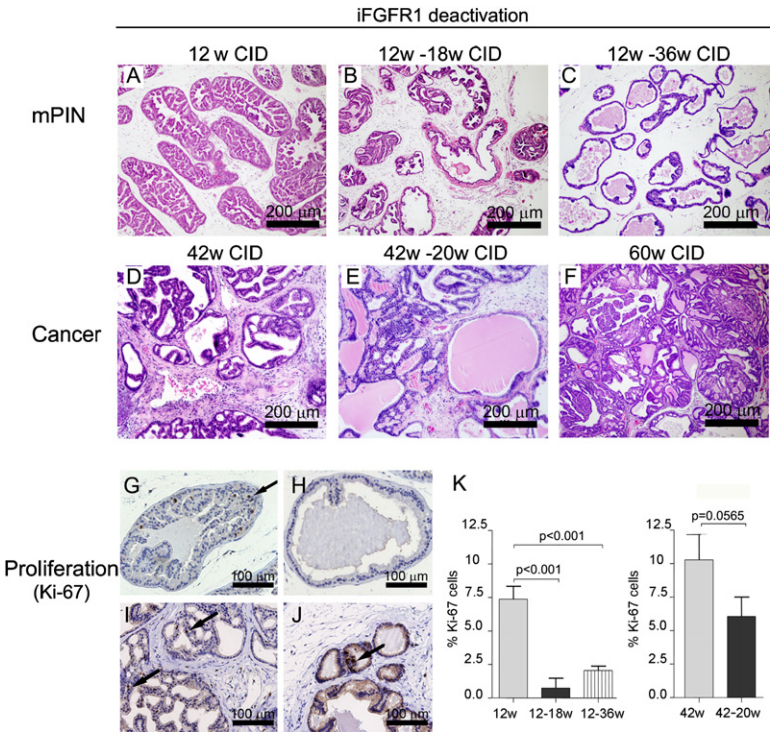

Figure 5. Deactivation of iFGFR1 Signaling by CID Withdrawal

(A–C) Reversibility of JOCK1 mPIN by 36 weeks. JOCK1 mice treated for 12 weeks with CID (A), followed by 18 and 36 weeks of CID withdrawal. Partial reversion of mPIN is seen after 18 weeks (B), and a complete reversion of JOCK1 mPIN to normal prostate is seen after 36 weeks of CID withdrawal (C).

(D–F) Deactivation of iFGFR1 in mice with PCa. (D) PCa seen after 42 weeks of CID. (E) JOCK1 prostates after 42 weeks CID treatment and 20 weeks of CID withdrawal. (F) JOCK1 treated for 68 weeks (F).

(G–J) Cellular proliferation measured by Ki-67 staining. JOCK1 mice treated for 12 weeks (G), 12 weeks on/18 weeks off (H), 42 weeks on (I), and 42 weeks on/20 weeks off (J).

(K) JOCK1 proliferating cell index shows a reduction following CID withdrawal at both mPIN ($p < 0.001$) and PCa ($p = 0.0565$) stages (t test, represented as mean ± SEM).

CID for 42 weeks followed by a 20-week washout period relative to 42-week treated JOCK1 mice, although the percentage of proliferating cells did not reach the basal levels seen when CID was removed from 12-week treated mice (Figure 5K). This reduction in cell proliferation could have accounted for the slower rate of cancer progression after drug withdrawal in comparison to JOCK1 mice treated beyond 42 weeks. Taken together, these results show that iFGFR1 plays a role in tumor initiation, progression, and maintenance, and even after PCa formation, iFGFR1 deactivation reduces tumor proliferation rates. Although difficult to quantitate, endogenous FGFR1 may partly compensate for loss of iFGFR1 signaling, masking some of the effects of iFGFR1 inhibition (Figure S3). These results demonstrate that FGFR1 signaling is sufficient to promote PCa and support the therapeutic targeting of FGFR1 as treatment, especially at earlier stages of PCa progression.

FGFR1 Drives Changes in Gene Expression that Are Linked to Human PCa

In order to identify genetic changes associated with iFGFR1-driven PCa progression, gene expression analysis was performed. The ability to synchronously activate iFGFR1 allowed us to examine gene expression changes at distinct stages of progression, including hyperplasia, mPIN, and PCa. This approach allowed us to determine which genes were enriched or selected as prostates became malignant and which genes were differentially expressed at various stages. Candidate gene lists were created by determining which molecules were over- or underexpressed in 3 of 4 conditions by 2-fold or higher with a p value and false discovery rate of less than 0.05 in comparison to wild-type mice. The cluster heat map of 977 misregulated genes contained several previously identified FGFR1 target molecules, such as *Mkp3/Dusp6* and *Spry1*, demonstrating specificity for iFGFR1 signaling (Figure 6A; Table S1).

Reduction in FGFR2iiib expression levels has been described for several cancers including PCa (Feng et al., 1997; Giri et al., 1999). Reassuringly, *Fgfr2* was one of the genes found to be downregulated. In order to further validate these results, primers that recognize exclusively the *Fgfr2iiib* isoform were designed for quantitative RT-PCR (qRT-PCR). Activation of FGFR1 for 6 and 24 hr after CID led to a five-fold decrease in *Fgfr2iiib* mRNA levels, indicating likely direct inhibition by iFGFR1 signaling (Figure 6B). Previous studies have shown that while FGFR2iiib levels are reduced in PCa progression, there is also an increase in the FGFR2iiic isoform that accompanies the overexpression of FGFR1 (Carstens et al., 1997; Feng et al., 1997). However, our results showed that after iFGFR1 activation there is no increase in *Fgfr2iiic* (data not shown), indicating that reduction of *Fgfr2iiib* levels is not due to alternative splicing.

There were also differences in the expression of several genes involved in the Wnt signaling pathway (Tables S1 and S2). Among these, the Wnt pathway receptor frizzled 4 (*Fzd4*), a positive modulator of canonical Wnt signaling (Xu et al., 2004), was shown to be upregulated (Figure 6A). Validation by qRT-PCR revealed a 2-fold increase after 24 hr and about 5-fold after 24 weeks of iFGFR1 activity relative to wild-type animals (Figure 6C). Furthermore, the levels of Wnt inhibitor factor-1 (*Wif1*), a known repressor of Wnt signaling, began to decrease after 24 hr of FGFR1 activation (Figure 6C). The large increase in *Fzd4* levels

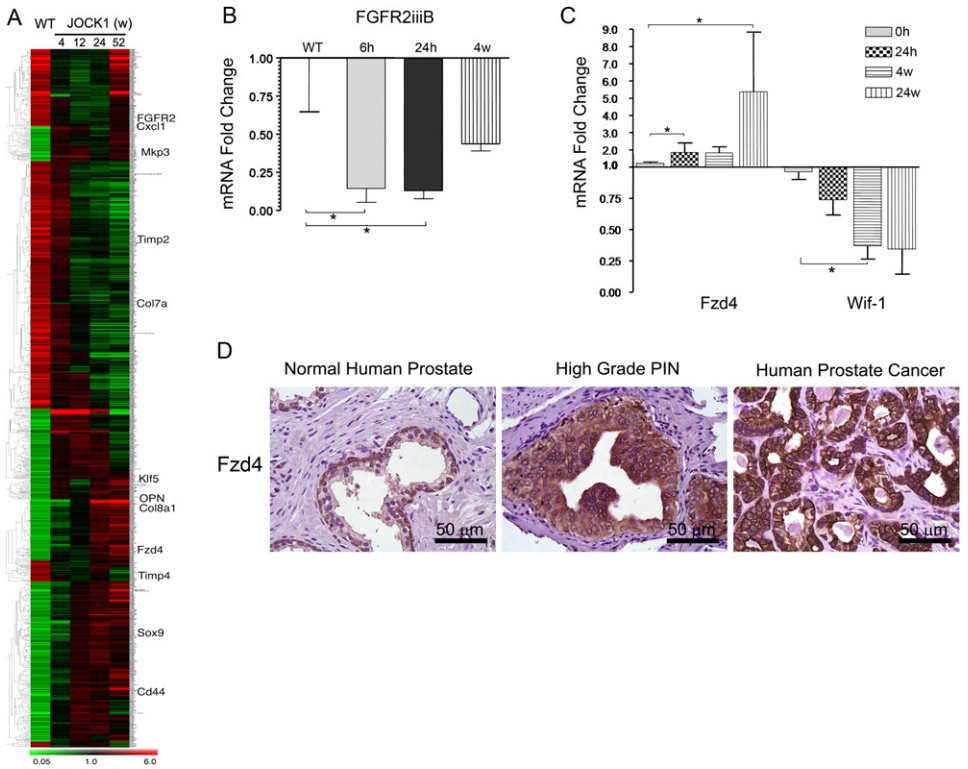

Figure 6. iFGFR1-Mediated Changes in Gene Expression

(A) Cluster heat map for the iFGFR1 gene expression profile at various stages of JOCK1 PCa progression, containing a total of 977 genes that were over- or underexpressed in 3 of 4 conditions by 2-fold or higher, with a p value and false discovery rate of less than 0.05 in comparison to wild-type mice.

(B) *Fgfr2iiib* mRNA levels measured by qRT-PCR (One-way ANOVA, $p < 0.05$, mean ± SEM).

(C) Validation for the expression levels of Wnt signaling members, *Fzd4* and *Wif1* (mean ± SEM, *$p < 0.05$).

(D) Expression of FZD4 in benign prostate, HG PIN, and prostate cancer. Normal tissues showed weak staining of luminal epithelial cells in more than 90% of cases. HG PIN and cancer cells had moderate to strong cytoplasmic staining in more than 50% and 80% of cases, respectively. No staining of stromal cells was seen.

after 24 weeks and the continued decrease in *Wif1* levels implicate a role for the Wnt pathway in iFGFR1 tumor progression. To further determine if iFGFR1 changes in expression of these Wnt signaling members could help identify novel human PCa markers, we stained human tissue arrays for Fzd4 expression. Interestingly, both high-grade PIN and clinically localized prostate cancers express significantly elevated Fzd4 levels ($p < 0.001$ for both groups, Mann-Whitney Rank Sum test) based on the immunohistochemical staining scores (Figure 6D).

To determine which changes in gene expression differentiate early/reversible stages from advanced/nonreversible stages of JOCK1 PCa, individual gene lists were created after 4, 24, and 52 weeks of iFGFR1 activation. Genes that were misregulated at each time point were compared for molecules that overlap or differentiate the groups (Figure 7A and Table S3). Genes found to be misregulated at late mPIN (24 weeks) and adenocarcinoma (52 weeks) may play a role in the transition from late mPIN to PCa. One gene found to be overexpressed at these late stages was osteopontin (*Opn*/*Spp1*), a molecule linked to PCa and metastasis (Thalmann et al., 1999) (Figure 7B). Furthermore, a known OPN receptor, CD44, was also upregulated 10-fold after 24 hr of iFGFR1 activation (Figure 7B). Another set of genes expressed after 24 and 52 weeks was procollagen type genes: *Col1a*, *Col8a*, *Col3a1*, and *Col5a1* (Table S3). Collagen molecules have been linked to a desmoplastic response in PCa, a criteria linked to tumor invasion (Ayala et al., 2003). In order to validate these results, Masson's trichrome stain for collagen molecules was performed. An increase in new collagen deposition was apparent as indicated by blue staining after 24 weeks of iFGFR1 activation, leading to fibrosis after 52 weeks (Figure 7C). Taken together, these results provide a molecular gene signature for FGFR1-driven PCa progression with striking similarities with the human disease and may help to explain the difference in reversibility at various stages as well as indicating putative therapeutic target.

FGFR1 Leads to an Increase in EMT-Associated Sox9 Expression

In order to find potential molecules that could contribute to FGFR1-mediated EMT, we focused on direct iFGFR1

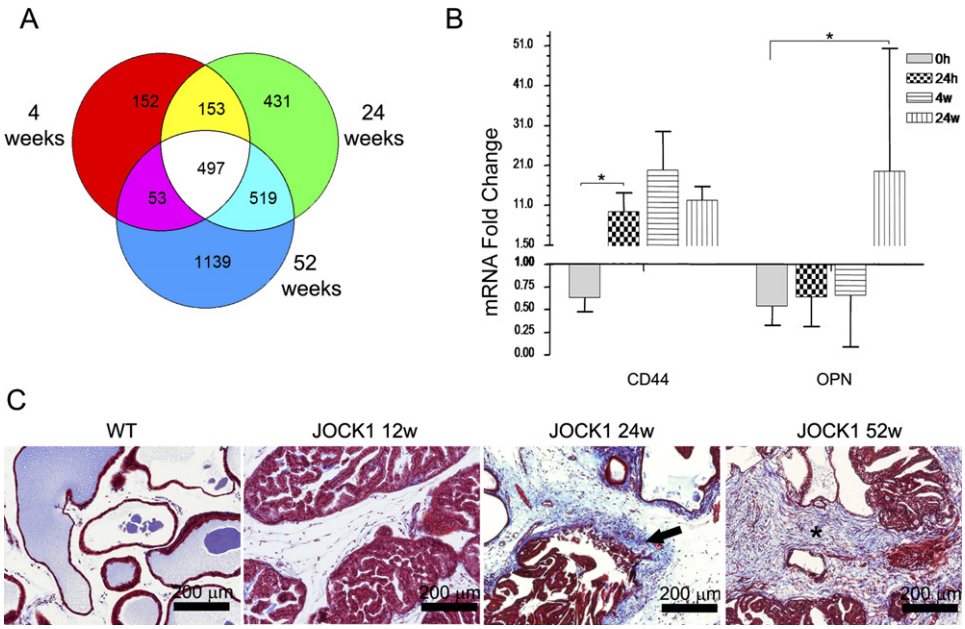

Figure 7. Comparison of Gene Expression at Distinct Stages of Tumor Progression

(A) Venn diagram from three different gene lists at various stages of iFGFR1 PCa progression: hyperplasia (4 weeks), mPIN (24 weeks), and PCa (52 weeks).

(B) Validation of results obtained from (A) for *Opn* and *CD44* genes. *Opn* was found to be overexpressed at later stages of JOCK1 PCa progression, while one of its receptors, *CD44*, is a direct target of iFGFR1 signaling. Data are represented as mean ± SEM, *$p < 0.05$.

(C) Masson's Trichrome stain to analyze collagen expression, which begins to increase after 24 weeks (arrow) leading to fibrosis (*).

target genes that have been correlated with an EMT. Gene expression profiling at 0, 6, and 24 hr after iFGFR1 activation (V.D.A., L.E.P., and D.M.S., unpublished data) revealed several genes linked to EMT and tumorigenesis. Among these, EMT-linked MMPs and TGFβ signaling axis members were found to be upregulated by FGFR1 (Thiery and Sleeman, 2006). Furthermore, the transcription factor *Sox9* was also found to be increased after 6 and 24 hr of FGFR1 activation (Figure 8A). Sox9 has been shown to be overexpressed in recurrent human PCa (Wang et al., 2007) and was also upregulated during JOCK1 tumor progression (Figure 6A). Moreover, relative to WT mice, iFGFR1-mediated PCa and sarcomas reflected higher nuclear Sox9 staining (Figure 8B). Sox9 was also found to be expressed in both liver and lymph node metastases (Figure 8C). Sox9 has been shown to act synergistically with Snail1 and Snail2 to promote EMT and to modulate both Snail1 and Snail2 expression (Cheung et al., 2005; Sakai et al., 2006). Similar to Snail1, Snail2/Slug is associated with EMTs and can reduce E-cadherin levels leading to a loss of cell-cell contact and increased migration (Bolos et al., 2003; Thiery, 2002). Snail1 and -2 were also found to be expressed in JOCK1 metastases (Figure 8C), which were E-cadherin-deficient. Finally, we detected the coexpression of Sox9 and vimentin in metastatic lesions (Figure 8D). Thus, increased expression of Sox9 by iFGFR1 in prostate cells may participate in a tumorigenic EMT and metastasis.

DISCUSSION

It has remained controversial whether ectopic changes in FGFR1 expression and activity are a cause or a secondary effect of PCa progression. Previously reported prostate GEM models, which ectopically express FGF ligands, FGF3 or FGF8b, or constitutively active FGFR1, exhibit cellular hyperplasia and mPIN, but not apparently invasive adenocarcinoma (Chua et al., 2002; Wang et al., 2004; Song et al., 2002). Interestingly, whereas *Pten*$^{+/-}$ mice only progress to mPIN, cooperation of both FGF8b overexpression and *Pten* haploinsufficiency leads to PCa after loss of *Pten* heterozygosity (Zhong et al., 2006), consistent with a role of the FGF axis in PCa. In contrast, we demonstrate that prolonged iFGFR1 activity is sufficient to drive initiation and step-wise progression to invasive adenocarcinoma with complete penetrance by 42 weeks. There are several possible explanations for the divergent results of previous FGFR1 models and ours. One possibility is that the iFGFR1 allele may provide more efficient receptor oligomerization than so-called "constitutive" receptors. Moreover, the intermittent crosslinking achieved by biweekly CID may better reflect the cyclical activation of receptors seen in vivo that are responsive to diurnal changes in hormones, redox levels and proinflammatory cofactors.

JOCK1 mice displayed an increase in spindle-shaped cells, including sarcomas and lesions with features of both carcinomas and sarcomas (known as "sarcomatoid-carcinomas"), suggestive of an EMT. FGFR1 also

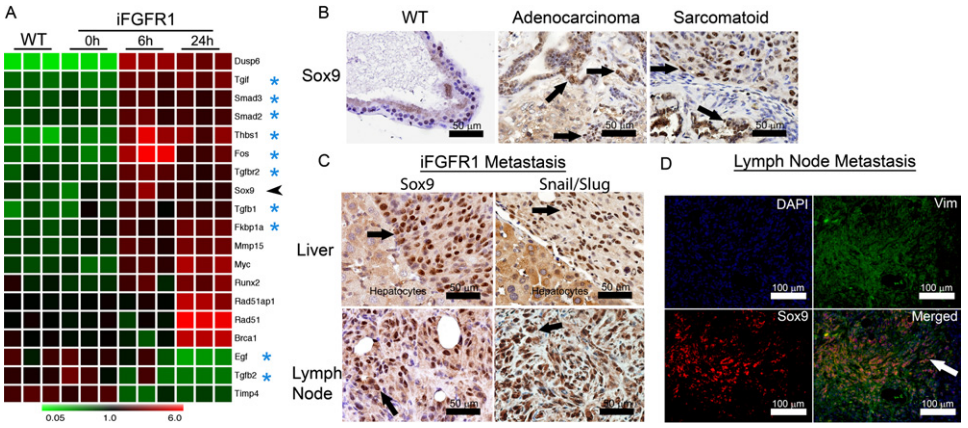

Figure 8. iFGFR1 Increases EMT-Associated Transcription Factor Sox9

(A) Cluster heat map of direct targets of iFGFR1 after 0, 6, and 24 hr of activation show an increase in genes that can contribute to FGFR1 tumorigenic-EMT, such as *Sox9* (arrowhead), TGFβ (*) signaling, and *MMP15*.

(B) IHC for Sox9 shows an increase nuclear expression in iFGFR1 tumors and sarcomas in comparison to WT.

(C) High Sox9 expression in iFGFR1 metastases. Metastatic lesions also exhibited an increase in Snail1/Snail2 staining.

(D) Coexpression of Sox9 (red) and Vim (green) in lymph node metastasis.

plays a crucial role in embryonic development by orchestrating an EMT (Ciruna and Rossant, 2001). In cancer, EMT has been proposed as a mechanism for the observed epithelial cell invasion and metastasis as cell motility is increased. One possible molecular link between FGFR1 and an EMT is increased Sox9 levels, which is overexpressed in recurrent PCa and can augment AR levels (Wang et al., 2007). Sox9 also can promote both *Snail* and *Slug* transcription and can physically interact with Slug to promote Slug's transcription in a feed-forward loop (Cheung et al., 2005; Sakai et al., 2006). Additionally, FGF2 has been shown to stimulate Sox9 expression via the MAPK pathway (Murakami et al., 2000). Taken together, iFGFR1 may trigger an EMT by activating the MAPK pathway, which increases Sox9 and, in turn, Snail2, potentiating invasion and metastasis.

What constitutes a true EMT, however, is highly contentious. Cells morphologically resembling mesenchymal cells do not always express known mesenchymal markers (Tarin et al., 2005) and may revert back to epithelial cells in a process described as a mesenchymal-to-epithelial transition. Therefore, identifying such events, especially in vivo, may prove particularly difficult due to its transient nature. An increase in mesenchymal cells can also occur following prostate epithelial-targeted pRb deletion, which leads to an expansion of fibroblast with reduced p53 levels (Hill et al., 2005). One possibility for these stromal changes may be the slight "off-target" ARR_2PB promoter leakiness, since the spindle-shaped cells we observe express high levels of AR. However, when the ARR_2PB promoter was used in ("EZC2-Prostate") reporter mice, bioluminescence and luciferase expression was observed almost exclusively within prostate epithelial cells and some associated tissues, but was orders of magnitude lower in distant organs, arguing for high specificity (Seethammagari et al., 2006). Independently, other mouse models that have used this promoter to target mitogenic oncogenes, such as c-Myc or constitutively active caFGFR1, to the prostate do not reveal a rapid increase in mesenchymal cells (Ellwood-Yen et al., 2003; Wang et al., 2004). Although paracrine signals from iFGFR1 epithelium could also lead to mesenchymal cell proliferation, our results clearly provide evidence for an EMT event, since invasive cells retain several epithelial markers and coexpress both epithelial and mesenchymal markers. Also, the appearance of these mesenchymal cells is synchronous with the development of invasive adenocarcinoma. Thus, our results clearly suggest that potent iFGFR1 signaling can lead to epithelial cell plasticity and an EMT in PCa progression.

Due to their highly enzymatic activity, diverse functions, and oncogenic potential, FGFR1 and other RTKs make good targets for cancer therapy (Skorski, 2002). One advantage of the CID system is that it can simulate FGFR1 inhibition by drug withdrawal, indicating whether growth factor signaling is necessary for tumor maintenance. Our results show that full reversibility of mPIN is possible by terminating iFGFR1 signaling. Thus, FGFR1 is sufficient for initiation, progression, and mPIN maintenance. In contrast, PCa continued to progress independent of iFGFR1 to a more aggressive adenocarcinoma, albeit at a slower rate than continually treated animals. Previous JOCK1-studies have shown that the initial hyperplastic changes prior to significant vascularization can be rapidly reversible after CID withdrawal due to a quick drop in cell proliferation and a potential increase in apoptosis (Freeman et al., 2003). Additionally, iFGFR1 can also promote neovascularization by increasing the proangiogenic factors HIF-1α, VEGF, and Ang-2 (Winter et al., 2007). However, unlike proliferation levels, maintenance of iFGFR1-mediated neovascularization is not fully dependent on constant signaling as shown after iFGFR1 inhibition, which leads to a slow and gradual decrease in JOCK1 vascularization. These results suggest that reductive remodeling in vascular architecture may be a rate-limiting step in JOCK1

mPIN and PCa regression. Taken together, these results propose a "susceptibility window" for FGFR1 target therapy, wherein patients may benefit most at early stages of PCa.

Since 52-week-old untreated JOCK1 mice were virtually identical to nontransgenic mice both phenotypically and genomically, there does not appear to be detectable CID-independent signaling by iFGFR1. Therefore, it is unclear how to reconcile continued PCa progression after CID withdrawal. One possibility is that endogenous FGFR1 could compensate for iFGFR1. Alternatively, as prostates become malignant, changes in the tumor microenvironment may establish new autocrine or paracrine signaling from epithelial-stroma interactions, sustaining tumor growth and vascularization. Due to differences between early PCa stages and late/nonreversible adenocarcinoma for both CID withdrawal and androgen ablation, we used gene expression microarrays to identify candidate genes that might distinguish these stages. Based on this approach, we observed that OPN, known to contribute to several biological processes, including proliferation and migration (Tuck et al., 1999; Thalmann et al., 1999), is expressed at later PCa stages, while OPN receptor, CD44, was rapidly induced by iFGFR1. This result mirrors studies in other PCa mouse models, in which OPN increases initially in mPIN and further in adenocarcinoma (Khodavirdi et al., 2006). Thus, the establishment of new autocrine and paracrine axes, such as OPN/CD44, as well as changes in tumor microenvironment found at later stages of JOCK-1 tumor progression, can help explain iFGFR1-independence.

Among other molecules identified by gene expression profiling, we found FGFR2iiib to be downregulated. FGFR2iiib is normally expressed by prostate epithelial cells, and its levels tend to be reduced in PCa, while FGFR1 (normally excluded from epithelial cells) increases (Naimi et al., 2002; Yan et al., 1993). Reintroduction of FGFR2 into PCa cells has been shown to reduce tumor growth, consistent with the lack of phenotypic changes we saw following 12-week activation of iFGFR2 (Feng et al., 1997; Freeman et al., 2003; Matsubara et al., 1998). Furthermore, depression of FGFR2 in the mouse prostate accelerates mPIN progression by caFGFR1 (Jin et al., 2003), while mice lacking *Fgfr2iiib* in the skin are more prone to papillomas and squamous cell carcinomas (Grose et al., 2007). Thus, FGFR2iiib can play a role as a tumor suppressor, and its loss has been proposed to be a required step in PCa progression (Carstens et al., 1997). Therefore, FGFR1 may also promote PCa by FGFR2 inhibition.

We also observed an increase in the expression of several Wnt axis members after iFGFR1 activation, including Fzd4, capable of inducing β-catenin (Xu et al., 2004). FZD4 is also significantly upregulated in human PCa and should serve as a prognostic indicator of disease. By contrast, the expression of the Wnt signaling repressor, *Wif1*, decreases after 4 weeks of iFGFR1 activity. Epigenetic silencing of *Wif1* in human cancer has been shown previously (Ai et al., 2006). In studies of human PCa, mRNA levels of *Wif1* were also seen to decrease, concomitant with *Fzd4* increase (Wissmann et al., 2003). Crosstalk between the FGF and Wnt pathways has been widely observed during development, such as during chick limb development (Kawakami et al., 2001). This interplay between FGF and Wnt has also been established for mammary tumorigenesis, leading to a synergistic selection in these two pathways and higher tumorigenicity (Kwan et al., 1992; MacArthur et al., 1995; Li et al., 2000). These results suggest that similar developmental events may provide a selective advantage in FGFR1-driven tumorigenesis.

In summary, we have shown that iFGFR1 signaling can promote an EMT, invasive adenocarcinoma and metastasis in an autochthonous model. Furthermore, this GEM prostate model may facilitate determination of which signaling pathways, like Wnt/β-catenin, complement FGFR1 activation. We have also shown that differences in sensitivity to FGFR1 inhibition at different stages of progression are indicative of a "susceptibility window," and underscore the broad utility of CID-mediated control of signaling molecules for optimizing treatment opportunities. Our results from gene expression profiling may prove particularly beneficial in validating molecules that not only play a role in the disease but complement FGFR1-independence. It will be of particular interest to determine whether therapies, such as antiangiogenesis, may complement FGFR1 inhibition and allow for reversion of prostate cancer.

EXPERIMENTAL PROCEDURES

Animals and Treatment

All mice were housed and treated at BCM's pathogen-free Transgenic Mouse Facility, according to regulatory standards as approved by the Institutional Animal Care and Use Committee. Generation and genotyping of JOCK1 mice has been described previously (Freeman et al., 2003). Mice were treated biweekly starting at 12 weeks of age by intraperitoneal injections of AP20187 (Ariad Pharmaceuticals, Cambridge, MA) at 2 mg/kg in drug diluent (16.7% propanediol, 22.5% PEG400, 1.25% TWEEN 80) or drug diluent alone.

Histology and Immunohistochemistry

The genitourinary (GU) tract of mice, comprised of bladder, seminal vesicles, urethra, and prostate lobes was removed and weighted. The ventral, dorsal lateral, and anterior lobes of prostates were dissected from the GU tract for fixing. All tissues were fixed in 10% neutral phosphate-buffered formalin, embedded in paraffin, and cut into 5 μm tissue sections, and hematoxylin and eosin staining was performed as previously described (Freeman et al., 2003).

Immunohistochemistry (IHC) analysis of 5 μm sections was performed by initial 55°C overnight incubation of slides, deparaffinization, and hydration. Antigen retrieval was performed using 10 mM sodium citrate buffer for 15 min. Antibody dilutions used were anti-androgen receptor 1:65 (Upstate, 06-680), anti-Snail 1:250 (Abcam, Ab17732), Sox9 (1607 Santa Cruz), and anit-Ki67 1:1000 (Novacastra, United Kingdom). For pan-cytokeratins 1:700 dilution (Dako, Z0622), antigen retrieval was performed using proteinase K at room temperature for 15 min. Endogenous peroxidases were quenched by incubating in 3% H_2O_2 for 15 min. Samples were then blocked for 1 hr using 10% goat serum followed by an overnight incubation with primary antibodies. After PBS-T washing, slides were incubated with biotinylated goat anti-rabbit (1:500) for 1 hr (1:300 for Snail). Stain was visualized by incubating with ABC for 45 min followed by DAB for 5 min (Vector Laboratories) and counterstain using hematoxylin.

IHC using mouse monoclonal antibodies was performed using a M.O.M. kit (Vector Labs). Antigen retrieval was performed using

10 mM sodium citrate (pH 6) for E-cadherin 1:500 and peroxidases were quenched using 3% H_2O_2 for 15 min. Blocking endogenous IgG receptors and subsequent steps were carried as described in the manufacturer's protocol.

Immunofluorescence and Double Staining

IF for SMA 1:200 (IA4, Dako) (no antigen retrieval) and p-Akt (9277S, Cell Signaling) was performed similarly to IHC but with substitution of ABC for streptavidin conjugated with Texas Red or FITC (Vector Lab), and counterstained with DAPI mounting media (Vector Lab).

Double staining was performed by deparaffinizing, hydrating in 100% and 95% EtOH steps, and rinsing sections in water. 10 mM sodium citrate antigen retrieval was performed, and endogenous IgG receptors were blocked for 1 hr (M.O.M. kit). Sections were incubated for 1 hr with anti-E-cadherin antibody 1:500 at 37°C, washed, and incubated for 1 hr at 37°C with anti-mouse IgG-rhodamine-conjugated antibody 1:100 (Santa Cruz Biotechnology, no. sc2084). Sections were washed and blocked for 1 hr with 5% donkey sera and incubated at 4°C overnight with anti-vimentin antibody (Santa Cruz, no. sc7557). After washing steps, sections were incubated with secondary anti-goat antibody at 1:100 (Santa Cruz, no. sc2084). Slides were counter stained with DAPI mounting media (Vector Lab). Digital pictures were taken using a Hamamatsu C9742-95 camera and processed using the Simple PCI software (Complex Inc.).

Pathological Grading

Histology slides stained by H&E were analyzed by two pathologists (M. Ittmann and G. Ayala) and graded from 0–3 for the extent of prostatic intraepithelial neoplasia (PIN), adenocarcinoma, transitional sarcomatoid lesions, and sarcoma. The average mean and standard deviation of both scores was taken to determine the distribution of phenotypes.

Proliferation Analysis

To determine the level of proliferation, five random high power fields of ventral prostate were examined per sample ($n \geq 5$ mice, except 18 week off [n = 3]). The total number of Ki-67 positive cells was divided by the total number of cells per power field, and the average of the five fields was used to determine the average mean and standard deviation.

Analysis of Prostate Cancer Tissues

Informed consent to use tissues for research was obtained by the Baylor Prostate Cancer SPORE Pathology Core under an IRB-approved protocol.

Statistical Analysis

One-way ANOVA and one-tailed unpaired t test analysis with graphical representation was performed using GraphPad Prism. Kruskal-Wallis analysis of variance (ANOVA) and Mann-Whitney tests were performed to identify significant differences in central tendencies of fold ratios for RT-PCR results.

Supplemental Experimental Procedures

Additional Experimental Procedures can be obtained in the Supplemental Data available with this article online.

Supplemental Data

The Supplemental Data include Supplemental Experimental Procedures, three supplemental figures, and three supplemental tables and can be found with this article online at http://www.cancercell.org/cgi/content/full/12/6/559/DC1/.

ACKNOWLEDGMENTS

We thank members of the Spencer lab, Jeffrey Rosen, Norman Greenberg, David Rowley and their labs for technical help, invaluable discussion, and reagents. This work was supported by NIH grant nos. U01-CA84296 (V.D.A., R.D.G., M.I., Y.Z., F.W., and D.M.S.), 1F31-GM069044 (V.D.A.), and P50CA058204 (M.I. and G.E.A.).

Received: May 2, 2007
Revised: September 3, 2007
Accepted: November 1, 2007
Published: December 10, 2007

REFERENCES

Ai, L., Tao, Q., Zhong, S., Fields, C.R., Kim, W.-J., Lee, M.W., Cui, Y., Brown, K.D., and Robertson, K.D. (2006). Inactivation of Wnt inhibitory factor-1 (WIF1) expression by epigenetic silencing is a common event in breast cancer. Carcinogenesis *27*, 1341–1348.

Ayala, G., Tuxhorn, J.A., Wheeler, T.M., Frolov, A., Scardino, P.T., Ohori, M., Wheeler, M., Spitler, J., and Rowley, D.R. (2003). Reactive stroma as a predictor of biochemical-free recurrence in prostate cancer. Clin. Cancer Res. *9*, 4792–4801.

Bolos, V., Peinado, H., Perez-Moreno, M.A., Fraga, M.F., Esteller, M., and Cano, A. (2003). The transcription factor Slug represses E-cadherin expression and induces epithelial to mesenchymal transitions: A comparison with Snail and E47 repressors. J. Cell Sci. *116*, 499–511.

Bradford, T.J., Tomlins, S.A., Wang, X., and Chinnaiyan, A.M. (2006). Molecular markers of prostate cancer. Urol. Oncol. *24*, 538–551.

Carstens, R.P., Eaton, J.V., Krigman, H.R., Walther, P.J., and Garcia-Blanco, M.A. (1997). Alternative splicing of fibroblast growth factor receptor 2 (FGF-R2) in human prostate cancer. Oncogene *15*, 3059–3065.

Cheung, M., Chaboissier, M.C., Mynett, A., Hirst, E., Schedl, A., and Briscoe, J. (2005). The transcriptional control of trunk neural crest induction, survival, and delamination. Dev. Cell *8*, 179–192.

Chua, S.S., Ma, Z.Q., Gong, L., Lin, S.H., DeMayo, F.J., and Tsai, S.Y. (2002). Ectopic expression of FGF-3 results in abnormal prostate and Wolffian duct development. Oncogene *21*, 1899–1908.

Ciruna, B., and Rossant, J. (2001). FGF Signaling Regulates Mesoderm Cell Fate Specification and Morphogenetic Movement at the Primitive Streak. Dev. Cell *1*, 37–49.

Ellwood-Yen, K., Graeber, T.G., Wongvipat, J., Iruela-Arispe, M.L., Zhang, J., Matusik, R., Thomas, G.V., and Sawyers, C.L. (2003). Myc-driven murine prostate cancer shares molecular features with human prostate tumors. Cancer Cell *4*, 223–238.

Feng, S., Wang, F., Matsubara, A., Kan, M., and McKeehan, W.L. (1997). Fibroblast growth factor receptor 2 limits and receptor 1 accelerates tumorigenicity of prostate epithelial cells. Cancer Res. *57*, 5369–5378.

Freeman, K.W., Welm, B.E., Gangula, R.D., Rosen, J.M., Ittmann, M., Greenberg, N.M., and Spencer, D.M. (2003). Inducible prostate intraepithelial neoplasia with reversible hyperplasia in conditional FGFR1-expressing mice. Cancer Res. *63*, 8256–8263.

Giri, D., Ropiquet, F., and Ittmann, M. (1999). Alterations in Expression of Basic Fibroblast Growth Factor (FGF) 2 and Its Receptor FGFR-1 in Human Prostate Cancer. Clin. Cancer Res. *5*, 1063–1071.

Grose, R., and Dickson, C. (2005). Fibroblast growth factor signaling in tumorigenesis. Cytokine Growth Factor Rev. *16*, 179–186.

Grose, R., Fantl, V., Werner, S., Chioni, A.M., Jarosz, M., Rudling, R., Cross, B., Hart, I.R., and Dickson, C. (2007). The role of fibroblast growth factor receptor 2b in skin homeostasis and cancer development. EMBO J. *26*, 1268–1278.

Hill, R., Song, Y., Cardiff, R.D., and Van Dyke, T. (2005). Selective Evolution of Stromal Mesenchyme with p53 Loss in Response to Epithelial Tumorigenesis. Cell *123*, 1001–1011.

Jemal, A., Siegel, R., Ward, E., Murray, T., Xu, J., and Thun, M.J. (2007). Cancer statistics, 2007. CA Cancer J. Clin. *57*, 43–66.

Jin, C., McKeehan, K., Guo, W., Jauma, S., Ittmann, M.M., Foster, B., Greenberg, N.M., McKeehan, W.L., and Wang, F. (2003). Cooperation between ectopic FGFR1 and depression of FGFR2 in induction of prostatic intraepithelial neoplasia in the mouse prostate. Cancer Res. *63*, 8784–8790.

Kawakami, Y., Capdevila, J., Buscher, D., Itoh, T., Esteban, C.R., and Belmonte, J.C.I. (2001). WNT Signals Control FGF-Dependent Limb Initiation and AER Induction in the Chick Embryo. Cell *104*, 891–900.

Khodavirdi, A.C., Song, Z., Yang, S., Zhong, C., Wang, S., Wu, H., Pritchard, C., Nelson, P.S., and Roy-Burman, P. (2006). Increased Expression of Osteopontin Contributes to the Progression of Prostate Cancer. Cancer Res. *66*, 883–888.

Kwabi-Addo, B., Ozen, M., and Ittmann, M. (2004). The role of fibroblast growth factors and their receptors in prostate cancer. Endocr. Relat. Cancer *11*, 709–724.

Kwan, H., Pecenka, V., Tsukamoto, A., Parslow, T.G., Guzman, R., Lin, T.P., Muller, W.J., Lee, F.S., Leder, P., and Varmus, H.E. (1992). Transgenes expressing the Wnt-1 and int-2 proto-oncogenes cooperate during mammary carcinogenesis in doubly transgenic mice. Mol. Cell. Biol. *12*, 147–154.

MacArthur, C., Shankar, D., and Shackleford, G. (1995). Fgf-8, activated by proviral insertion, cooperates with the Wnt-1 transgene in murine mammary tumorigenesis. J. Virol. *69*, 2501–2507.

Matsubara, A., Kan, M., Feng, S., and McKeehan, W.L. (1998). Inhibition of growth of malignant rat prostate tumor cells by restoration of fibroblast growth factor receptor 2. Cancer Res. *58*, 1509–1514.

Murakami, S., Kan, M., McKeehan, W.L., and de Crombrugghe, B. (2000). Up-regulation of the chondrogenic Sox9 gene by fibroblast growth factors is mediated by the mitogen-activated protein kinase pathway. Proc. Natl. Acad. Sci. USA *97*, 1113–1118.

Naimi, B., Latil, A., Fournier, G., Mangin, P., Cussenot, O., and Berthon, P. (2002). Down-regulation of (IIIb) and (IIIc) isoforms of fibroblast growth factor receptor 2 (FGFR2) is associated with malignant progression in human prostate. Prostate *52*, 245–252.

Ornitz, D.M., and Itoh, N. (2001). Fibroblast growth factors. Genome Biol. *2*, REVIEWS3005.

Ornitz, D.M., Xu, J., Colvin, J.S., McEwen, D.G., MacArthur, C.A., Coulier, F., Gao, G., and Goldfarb, M. (1996). Receptor specificity of the fibroblast growth factor family. J. Biol. Chem. *271*, 15292–15297.

Ozen, M., Giri, D., Ropiquet, F., Mansukhani, A., and Ittmann, M. (2001). Role of fibroblast growth factor receptor signaling in prostate cancer cell survival. J. Natl. Cancer Inst. *93*, 1783–1790.

Powers, C.J., McLeskey, S.W., and Wellstein, A. (2000). Fibroblast growth factors, their receptors and signaling. Endocr. Relat. Cancer *7*, 165–197.

Sakai, D., Suzuki, T., Osumi, N., and Wakamatsu, Y. (2006). Cooperative action of Sox9, Snail2 and PKA signaling in early neural crest development. Development *133*, 1323–1333.

Savagner, P., Valles, A.M., Jouanneau, J., Yamada, K.M., and Thiery, J.P. (1994). Alternative splicing in fibroblast growth factor receptor 2 is associated with induced epithelial-mesenchymal transition in rat bladder carcinoma cells. Mol. Biol. Cell *5*, 851–862.

Seethammagari, M.R., Xie, X., Greenberg, N.M., and Spencer, D.M. (2006). EZC-Prostate Models Offer High Sensitivity and Specificity for Noninvasive Imaging of Prostate Cancer Progression and Androgen Receptor Action. Cancer Res. *66*, 6199–6209.

Shappell, S.B., Thomas, G.V., Roberts, R.L., Herbert, R., Ittmann, M.M., Rubin, M.A., Humphrey, P.A., Sundberg, J.P., Rozengurt, N., Barrios, R., et al. (2004). Prostate pathology of genetically engineered mice: Definitions and classification. The consensus report from the Bar Harbor meeting of the Mouse Models of Human Cancer Consortium Prostate Pathology Committee. Cancer Res. *64*, 2270–2305.

Skorski, T. (2002). Oncogenic Tyrosine Kinases and the DNA-Damage Response. Nat. Rev. Cancer *2*, 351–360.

Song, Z., Wu, X., Powell, W.C., Cardiff, R.D., Cohen, M.B., Tin, R.T., Matusik, R.J., Miller, G.J., and Roy-Burman, P. (2002). Fibroblast growth factor 8 isoform B overexpression in prostate epithelium: A new mouse model for prostatic intraepithelial neoplasia. Cancer Res. *62*, 5096–5105.

Tarin, D., Thompson, E.W., and Newgreen, D.F. (2005). The Fallacy of Epithelial Mesenchymal Transition in Neoplasia. Cancer Res. *65*, 5996–6001.

Thalmann, G.N., Sikes, R.A., Devoll, R.E., Kiefer, J.A., Markwalder, R., Klima, I., Farach-Carson, C.M., Studer, U.E., and Chung, L.W.K. (1999). Osteopontin: Possible Role in Prostate Cancer Progression. Clin. Cancer Res. *5*, 2271–2277.

Thiery, J.P. (2002). Epithelial-Mesenchymal Transition in Tumor Progression. Nat. Rev. Cancer *2*, 442–454.

Thiery, J.P., and Sleeman, J.P. (2006). Complex networks orchestrate epithelial-mesenchymal transitions. Nat. Rev. Mol. Cell Biol. *7*, 131–142.

Tuck, A.B., Arsenault, D.M., O'Malley, F.P., Hota, C., Ling, M.C., Wilson, S.M., and Chambers, A.F. (1999). Osteopontin induces increased invasiveness and plasminogen activator expression of human mammary epithelial cells. Oncogene *18*, 4231–4246.

Wang, F., McKeehan, K., Yu, C., Ittmann, M., and McKeehan, W.L. (2004). Chronic activity of ectopic type 1 fibroblast growth factor receptor tyrosine kinase in prostate epithelium results in hyperplasia accompanied by intraepithelial neoplasia. Prostate *58*, 1–12.

Wang, H., McKnight, N.C., Zhang, T., Lu, M.L., Balk, S.P., and Yuan, X. (2007). SOX9 is expressed in normal prostate basal cells and regulates androgen receptor expression in prostate cancer cells. Cancer Res. *67*, 528–536.

Winter, S.F., Acevedo, V.D., Gangula, R.D., Freeman, K.W., Spencer, D.M., and Greenberg, N.M. (2007). Conditional activation of FGFR1 in the prostate epithelium induces angiogenesis with concomitant differential regulation of Ang-1 and Ang-2. Oncogene *26*, 4897–4907.

Wissmann, C., Wild, P.J., Kaiser, S., Roepcke, S., Stoehr, R., Woenckhaus, M., Kristiansen, G., Hsieh, J.C., Hofstaedter, F., Hartmann, A., et al. (2003). WIF1, a component of the Wnt pathway, is down-regulated in prostate, breast, lung, and bladder cancer. J. Pathol. *201*, 204–212.

Xian, W., Schwertfeger, K.L., Vargo-Gogola, T., and Rosen, J.M. (2005). Pleiotropic effects of FGFR1 on cell proliferation, survival, and migration in a 3D mammary epithelial cell model. J. Cell Biol. *171*, 663–673.

Xu, Q., Wang, Y., Dabdoub, A., Smallwood, P.M., Williams, J., Woods, C., Kelley, M.W., Jiang, L., Tasman, W., Zhang, K., and Nathans, J. (2004). Vascular development in the retina and inner ear: Control by Norrin and Frizzled-4, a high-affinity ligand-receptor pair. Cell *116*, 883–895.

Yan, G., Fukabori, Y., McBride, G., Nikolaropolous, S., and McKeehan, W.L. (1993). Exon switching and activation of stromal and embryonic fibroblast growth factor (FGF)-FGF receptor genes in prostate epithelial cells accompany stromal independence and malignancy. Mol. Cell. Biol. *13*, 4513–4522.

Li, Y., Hively, W.P., and Varmus, H.E. (2000). Use of MMTV-Wnt-1 transgenic mice for studying the genetic basis of breast cancer. Oncogene *19*, 1002–1009.

Zhang, J., Thomas, T.Z., Kasper, S., and Matusik, R.J. (2000). A small composite probasin promoter confers high levels of prostate-specific gene expression through regulation by androgens and glucocorticoids in vitro and in vivo. Endocrinology *141*, 4698–4710.

Zhong, C., Saribekyan, G., Liao, C.-P., Cohen, M.B., and Roy-Burman, P. (2006). Cooperation between FGF8b Overexpression and PTEN Deficiency in Prostate Tumorigenesis. Cancer Res. *66*, 2188–2194.

Zhou, B.P., Deng, J., Xia, W., Xu, J., Li, Y.M., Gunduz, M., and Hung, M.-C. (2004). Dual regulation of Snail by GSK-3[beta]-mediated phosphorylation in control of epithelial-mesenchymal transition. Nat. Cell Biol. *6*, 931–940.

Accession Numbers

Microarray data are available at http://www.ebi.ac.uk/microarray-as/aer/entry (Accession number E-MEXP-1296).